Applied Catalysis B: Environmental 185 (2016) 295–306

Contents lists available at ScienceDirect

Applied Catalysis B: Environmental

journal homepage: www.elsevier.com/locate/apcatb

Immobilization of self-stabilized plasmonic Ag-AgI on mesoporous Al_2O_3 for efficient purification of industrial waste gas with indoor LED illumination

Dehua Xia[a,c], Lingling Hu[a], Xiuqin Tan[a], Chun He[a,*], Wenqi Pan[a], Tushi Yang[a], Yanling Huang[a], Dong Shu[b,*]

[a] School of Environmental Science and Engineering, Sun Yat-sen University, Guangzhou 510275, China
[b] Key Lab of Technology on Electrochemical Energy Storage and Power Generation in Guangdong Universities, School of Chemistry and Environment, South China Normal University, Guangzhou 510006, China
[c] Department of Civil and Environmental Engineering, The Hong Kong University of Science and Technology, Clear Water Bay, K.L., Hong Kong, China

ARTICLE INFO

Article history:
Received 17 September 2015
Received in revised form
10 December 2015
Accepted 11 December 2015
Available online 14 December 2015

Keywords:
Plasmonic Ag-AgI/Al_2O_3
NO removal
Wet impregnation-precipitation
Photocatalytic activity
Industrial waste gas

ABSTRACT

The immobilization of a photocatalyst on a proper support is pivotal for practical environmental applications. In this work, the plasmonic Ag-AgI with photoinduced self-stability was successfully immobilized on mesoporous Al_2O_3 by a wet impregnation-precipitation and in-situ photoreduction method. The immobilized Ag-AgI/Al_2O_3 was applied for photocatalytic removal of ppm-leveled NO under illumination of indoor LED tubes, which could obtain 100% NO removal in minutes at optimized conditions. The large dispersion of Ag-AgI on mesoporous Al_2O_3 was firmly enough to overwhelm the continuous air flowing, and the enlarged surface area of Ag-AgI could efficiently enhance NO removal efficiency than pure Ag-AgI powder. Most importantly, the plasmonic Ag-AgI/Al_2O_3 was stable in activity and can be used repeatedly without deactivation. On the basis of reactive species trapping and reaction intermediate monitoring, the responsible reactive species of photogenerated $^{\bullet}OH$, $^{\bullet}O_2^-$, H_2O_2 and h^+ were confirmed and the possible reaction mechanism of photocatalytic NO oxidation by Ag-AgI/Al_2O_3 was revealed. The present work could provide new perspectives for promoting large-scale environmental applications of supported plasma photocatalysts.

1. Introduction

Nitrogen oxides (NO_x), which result from automobile exhaust gas and industrial combustion of fossil fuels, are a major source of air pollution and cause ozone depletion, acid rain and photochemical smog [1,2]. This has serious implications on the environment and health of the mankind [3,4]. Among the NO_x emitted from stationary combustion sources, more than 90% of NO_x is nitric oxide (NO). Till now, many conventional techniques have been developed to eliminate NO in industrial emission, including selective catalytic reduction (SCR), wet scrubbing, physical adsorption, biofiltration, catalytic decomposition and thermal catalysis methods [5–8]. However, these technologies were not economically feasible for removal of air pollutants at the parts per million (ppm) levels, as some of them need large occupying area or high operating costs, even the occurrence of post-disposal and regeneration problems [5–8]. Therefore, the ideal process should be developed with further decreasing the economic and environmental costs of potential secondary pollution.

Visible light driven (VLD) photocatalysis as a green technology that could use natural sunlight or artificial light to purify air pollutants at ambient condition, provides an attractive alternative to conventional approaches. Several VLD photocatalysts have been prepared and applied for enhanced NO removal, such as doped TiO_2, BiOX, Bi_2WO_6, $In(OH)_xS_y$, NiO, hematite, C_3N_4 [9–15]. However, these photocatalysts are usually used in powdery form without immobilization on a proper support and the utilization are only limited at ppb-level of indoor air.

Currently, the localized surface plasmon resonance (SPR) effect of noble-metal nanoparticles (e.g. Ag, Au, Pt) has become a research focus in the development of VLD photocatalysts [16–23]. The VLD activity of plasmonic photocatalyst is originated from the distinctive plasmon resonance effect, which induced by the collective

* Corresponding authors at: School of Environmental Science and Engineering, Sun Yat-sen University, Guangzhou 510275, China.
E-mail addresses: hechun@mail.sysu.edu.cn (C. He), dshu@scnu.edu.cn (D. Shu).

http://dx.doi.org/10.1016/j.apcatb.2015.12.019
0926-3373/

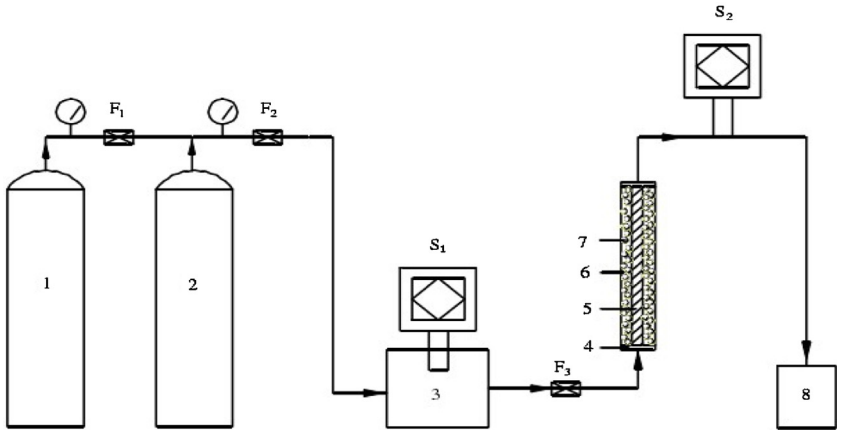

Fig. 1. Schematic diagram of photocatalytic removal of NO. 1, NO gas cylinder; 2, N_2 gas cylinder; 3, inlet mixing box; 4, sparger; 5, visble light source (LED tube); 6, Pyrex glass reactor; 7, Ag-AgI/Al_2O_3 photocatalyst; 8, outlet; F1–F3, gas flow meters; S1–S2, gas sensors.

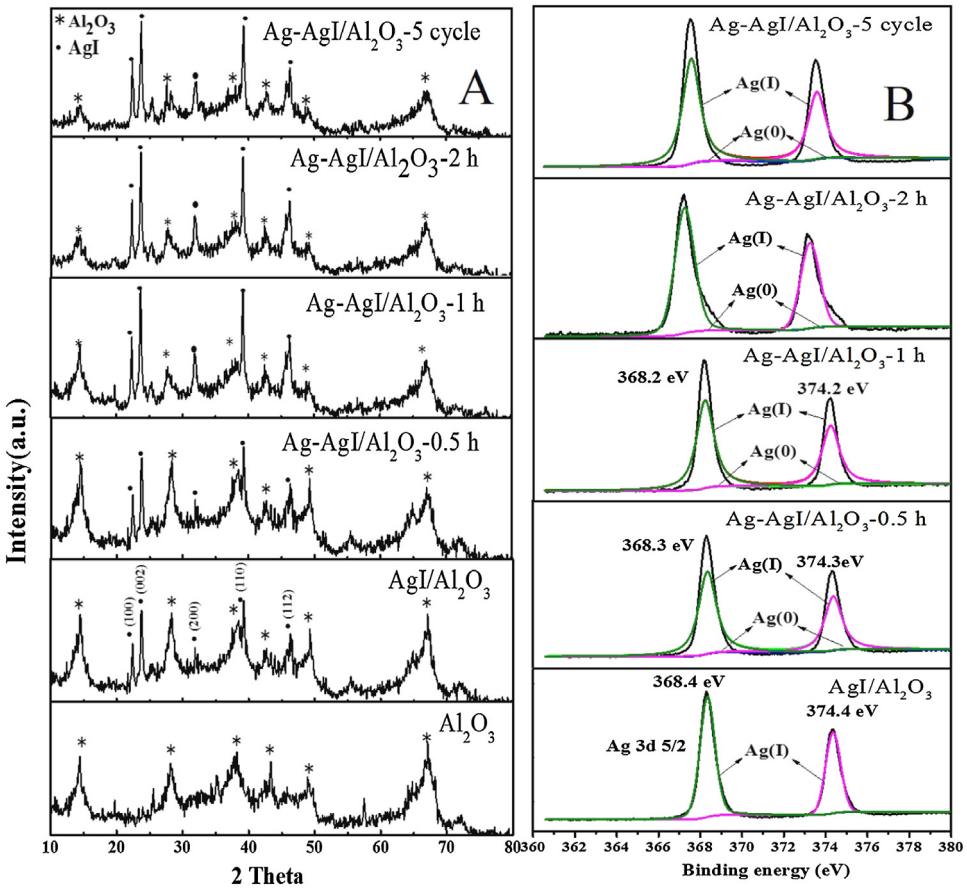

Fig. 2. XRD pattern (A) and XPS spectra of Ag 3d (B) in pure Al_2O_3, AgI/Al_2O_3, Ag-AgI/Al_2O_3 irradiated for 0.5 h, 1 h, 2 h, and used Ag-AgI/Al_2O_3 after 5 cycles.

oscillations of surface electrons from noble-metal nanoparticles. By far, many kinds of plasmonic photocatalyst have been developed and efficiently utilized for environmental remediation, such as Ag/AgX (X = Cl, Br) [16,17], Ag/AgBr/TiO_2 [18], Ag/AgBr/Bi_2WO_6 [20], Ag/AgX/CNTs [21], Ag@AgCl/graphene [19,22], and Ag-AgBr-C_3N_4 [23], etc. Despite these promising results, the utilization of plasmonic Ag-AgX is controversial mainly questioning on its stability during photocatalytic reactions. Interestingly, many research found that photosensitive AgX can transform into a stable Ag-AgX photocatalyst after in situ formation of partial Ag on the surface of AgX nanoparticles [17,23–27]. Motivated by this, loading stabilized Ag/AgX onto a suitable supporting material may provide an ideal solution for removal of NOx at ppm-level in industrial waste gas. For practical application, the powdery photocatalyst would be simply blown away and time-consuming for nano-photocatalysts recycle. Therefore, to apply photocatalytic techniques in waste gas purification, it is essential to develop a facile process to effectively immobilize the powdery photocatalyst on a proper support [28]. To our knowledge, the charge transfer processes of plasmonic induced charges and the mechanism of NO removal on immobilized plasmonic photocatalyst has not been reported yet.

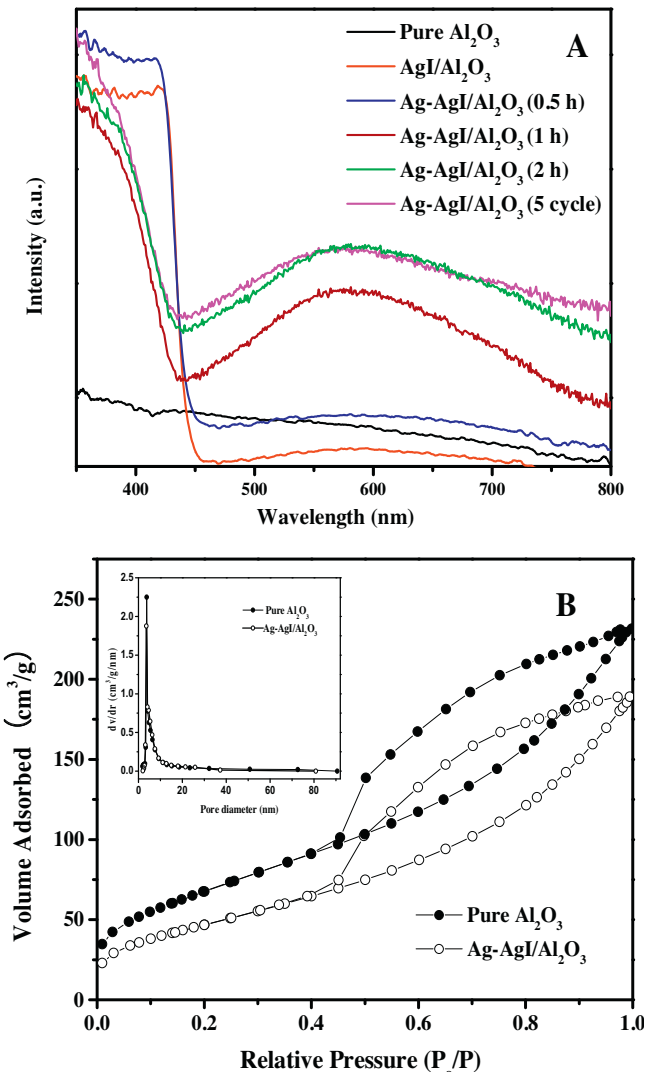

Fig. 3. (A) UV–vis diffuse reflectance spectra of pure Al_2O_3 and Ag-AgI/Al_2O_3 irradiated with 0.5 h, 1 h, 2 h; (B) N_2 adsorption and desorption isotherms and corresponding pore-size distribution curves (inset) for pure Al_2O_3 and Ag-AgI/Al_2O_3.

Table 1
Composition (atom%) of Ag species in immobilized Ag-AgI/Al_2O_3 according to XPS analysis.

Sample	Ag^0	Ag^+
AgI/Al_2O_3	0.015	0.747
Ag-AgI/Al_2O_3 (after 0.5 h)	0.106	0.659
Ag-AgI/Al_2O_3 (after 1 h)	0.163	0.602
Ag-AgI/Al_2O_3 (after 2 h)	0.166	0.602
Ag-AgI/Al_2O_3 (after 5 cycle)	0.168	0.601

Note: The amount of metallic Ag is calculated from the atom ratio of Ag: I, on the basis of AgI formula.

A plasmonic photocatalyst is described herein consisting of Ag-AgI were immobilized on mesoporous Al_2O_3, using the deposition-precipitation and concessive photoreduction method. The great dispersion of self-stabilized Ag-AgI on Al_2O_3 was firmly enough to overwhelm the continuous flowing air, owing to the mesporous architecture supports. The stabilizing process and microstructure change of the Ag-AgX were investigated accordingly. At optimal condition, Ag-AgI/Al_2O_3 showed an exceptionally high NO removal ratio of 100% under real indoor illumination of white LED tubes. The reaction mechanism of photocatalytic removal of NO with Ag-AgI/Al_2O_3 was revealed on the basis of scavenger study and reactive oxygen species (ROSs) determination. The present investigation demonstrated that a self-stabilized plasmonic Ag-AgI could be immobilized by a simple and economical process for efficient purification of NO at ppm-level in waste gas under LED irradiation, which could promote the practical environmental application of plasma photocatalyst.

2. Experimental

2.1. Chemicals and materials

All chemicals were analytical grade and were used without any further purification. $AgNO_3$ and KI with analytical grade were purchased from Guangdong Guanhua Chemical Co., Ltd. China. Aluminium oxide activated (Al_2O_3) was purchased from Sinopharm Chemical Reagent Co., Ltd. NO gas source with a traceable concentration of 2000 ppm in N_2 was supplied from Foshan Gao Neng Da Chemical Industry Co., Ltd, China. Deionized water was used throughout this study. Scavenger stock solutions: 1.0 M isopropanol (Riedel-de Haën®, Germany) for $^{\bullet}OH$, 1.0 M $K_2Cr_2O_7$ (Merck, Germany) for e^-, 1.0 M sodium oxalate (Fuchen, China) for h^+, 100 mM Fe(II)-EDTA for H_2O_2 (prepared with $FeSO_4$ and Na_2EDTA, Ajax Chemicals, Australia), 100 mM TEMPOL (Fuchen, China) for $^{\bullet}O_2^-$ [29–32].

2.2. Preparation of Ag-AgI/Al_2O_3 photocatalyst

Ag-AgI/Al_2O_3 photocatalysts were prepared by wet impregnation-precipitation and following photoreduction method [17]. Firstly, 40 g Al_2O_3 particles were impregnated into 100 ml 0.05 M $AgNO_3$ solution with constant stirring 30 min. Then, these prepared Al_2O_3 spheres were transferred into 100 ml 0.05 M KI solution with constant stirring 30 min. Meantime, the precipitated Ag^+ reacted with I^- to form AgI on the surface of mesoporous Al_2O_3. Then, the catalyst was immersed with deionized water and irradiated with visible light ($\lambda > 400$ nm) for 0.5 h, 1 h, 2 h to reduce adsorbed AgI to self-stable Ag/AgI photocatalyst. Finally, the resulting samples were washed several times with deionized water and dried at 393 K for 12 h in an oven. In contrast, Ag-AgI/ZSM-5 (Zeolite Socony Mobil-5), Ag-AgI/ZSM-4 and Ag-AgI/Zeolite catalysts were also prepared with the same method.

2.3. Characterization of Ag-AgI/Al_2O_3 photocatalyst

Self-stabilized Ag-AgI/Al_2O_3 were carried out using an X-ray diffractometer (XRD, D-MAX 2200 VPC, Japan) with radiation of Cu target (Kα, $\lambda = 1.54059$ Å). The content of elements in Ag-AgI/Al_2O_3 photocatalyst was determined by energy-dispersive spectroscopy (EDS, Quanta 400F, Holland) and X-ray photoelectron spectroscopy (XPS, KRATOA XSAM800, Japan). Specific BET surface area and pore size distribution were determined with an Autosorb-1-C Chemisorption/Physisorption Analyzer (Quantachrome, USA) by nitrogen adsorption and desorption at 77.3 K. UV–vis diffuse reflectance spectra (UV–vis DRS) of samples were recorded on a spectrophotometer (Shimadzu UV-PC3101PC) with an integrating sphere (Specular Reflectance ATT.5DEG). The photoelectrochemical measurements for catalyst were performed using an IM6ex electrochemical workstation (Zahner, Germany) with a standard three-electrode assembly. Furthermore, the electrochemical impedance spectroscopy (EIS) measurements were carried out using a potentiostat/galvanostat (Autolab, PGSTAT302N) coupled to a lock-in amplifier (PGSTAT 302N).

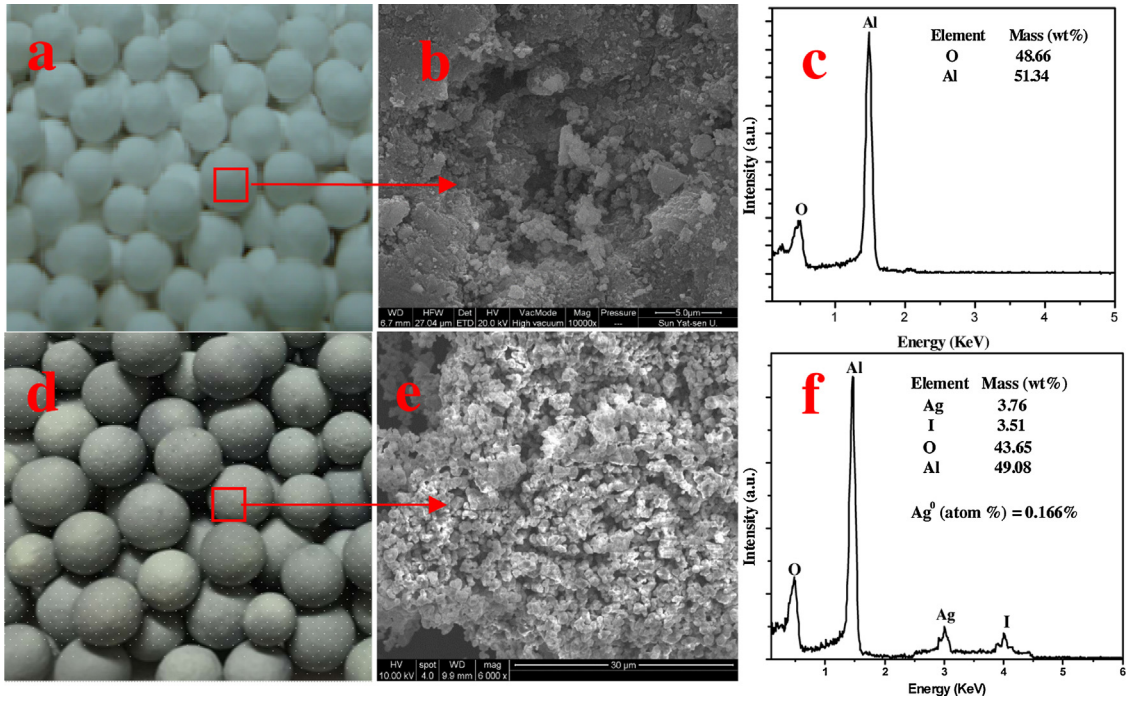

Fig. 4. Photos, SEM images and EDS spectrums of pure Al_2O_3 (a–c) and Ag-AgI/Al_2O_3 irradiated after 2 h (d–f).

2.4. Plasma induced photocatalytic removal of NO

The photocatalytic removal of NO at ppm levels by Ag-AgI/Al_2O_3 were carried out in a continuous flow reactor at ambient temperature (Fig. 1). The photocatalytic reactor with a size of 2.0 cm in diameter and 60 cm height was made of Pyrex glass. A 10 W white or green LED tube (Shanghai Aojia Lighting Appliance Co. Ltd.), was vertically placed inside the reactor, whose light spectrum were shown in Fig. S1. For each experiment, different amount of as-prepared Ag-AgI/Al_2O_3 were padded in the reactor. The initial concentration of NO was diluted to be 50 ppm by the air stream. The gas streams were premixed completely in a mixing box by a fan and the inlet velocity was controlled at 0.08 L min^{-1} by a mass flow controller. NO sensor (S_1, S_2) (Detcon, DM−100-NO) were installed to continuously monitor the inlet and outlet of NO concentration. NO was introduced into the reactor through a sparger, after the adsorption–desorption equilibrium between gas molecular and photocatalysts was achieved, the lamp was turned on. The removal ratio (η) of NO was calculated as $\eta\,(\%) = (1 - C/C_0) \times 100\%$, where C and C_0 are concentrations of NO in the outlet steam and feeding stream, respectively.

3. Results and discussion

3.1. Characterization of photoinduced self-stabilized Ag-AgI/Al_2O_3

To study the stabilizing process of Ag-AgI/Al_2O_3, the effect of photoreduction time on the stability of AgI/Al_2O_3 was analyzed through XRD firstly. As shown in Fig. 2A, the XRD patterns of Ag-AgI/Al_2O_3 with different irradiation time (0.5–2 h) are almost identical with AgI/Al_2O_3, all exhibited coexistent phases of both AgI and Al_2O_3 except for the substrate peaks of Al_2O_3, peaks at $2\theta = 22.319$, 23.707, 39.204, and 46.308 °C can be well indexed to the hexagonal β-AgI phase (JCPDS No.09-0374) [17,23]. These results clearly indicate that the crystalline AgI was formed on mesoporous Al_2O_3 and AgI phase still maintained well even after light irradiation. Notably, there is no observation of diffraction peaks assigned to metallic Ag even for sample after 2 h irradiation, which is presumably due to the small particle size and high dispersion of metallic Ag [17,23].

To further study the formation of metallic Ag on the surface of AgI/Al_2O_3, the samples were analyzed by XPS spectra (Fig. 2B) and UV–vis DRS (Fig. 3A). As shown in Fig. 2B, two bands at 367.2 and 373.0 eV were observed, which can be ascribed to Ag 3d5/2 and Ag 3d3/2 binding energies, respectively. Moreover, the divided bands at 367.2 and 373.0 indicate the presence of Ag(I), whereas bands at 368.0 and 374.0 eV suggest the existence of the metallic Ag(0). DRS results showed that the mesoporous Al_2O_3 was almost no response at wavelengths between 200 and 800 nm, while AgI/Al_2O_3 exhibit the strong response in the ultraviolet (UV) region but weak absorption tail in the VL region with a characteristic excitation peak at 425 nm, in accordance with the reported pure AgI [17,23,25]. After photoreduction for 0.5 h, it can be seen AgI/Al_2O_3 samples began to exhibit a low VL absorption in 450–800 nm region, which is attributed to the plasmonic resonance absorption of metallic Ag [17]. The XPS result analysis indicated that there is a small amount occurrence of metallic Ag (ca. 0.106%) (Table 1). Nevertheless, further prolonged irradiation time from 1 h to 2 h, the intensity of the plasmonic absorption at 450–800 nm for samples has no obvious change, presumably suggesting the size and number of metallic Ag are almost becoming stable [17,24]. The corresponding XPS results further confirmed this, as the amount (ca. 0.163–0.168% in Table 1) of the metallic Ag does not further increase, consistent with UV–vis results.

Therefore, the above results strongly demonstrate that Ag-AgI/Al_2O_3 samples can obtain photoinduced self-stability after 1 h VL irradiation, i.e. instable AgI can be transformed into a stable Ag-AgI after in-situ formation of partial Ag on AgI surface. In the initial photoreduction time, the photogenerated electrons are preferably transferred to the surface lattice Ag^+ in AgI. However, once a certain amount of metallic Ag is formed on AgI surface, the following photogenerated electrons will prefer to transfer to the metallic Ag sites and then are captured by oxygen, therewith Ag-AgI became stable accordingly [17,23,25]. The BET specific area and pore-size distri-

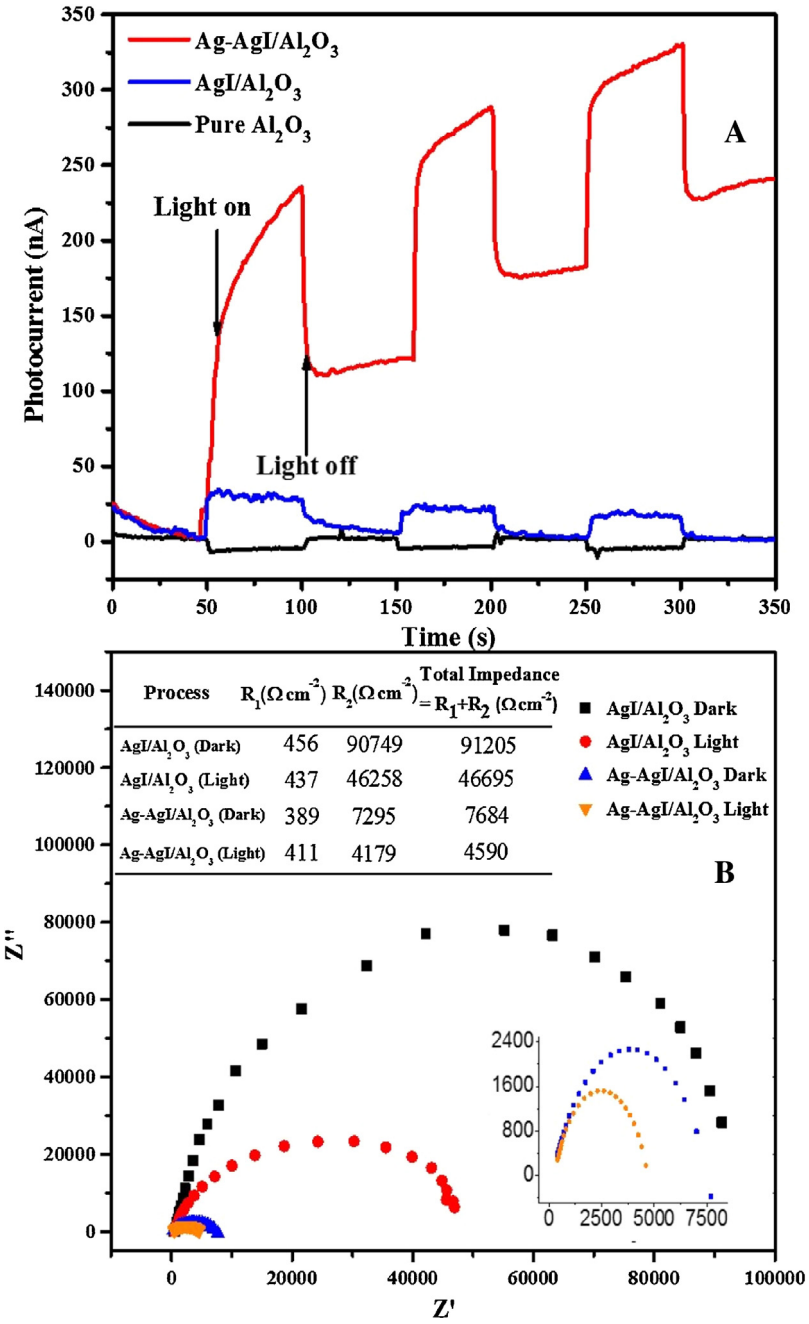

Fig. 5. (A) Photocurrent generation on Al_2O_3, AgI/Al_2O_3 and Ag-AgI/Al_2O_3 electrodes under VL irradiation; (B) electrochemical impedance spectroscopy (EIS) Nyquist impedance plots of AgI/Al_2O_3 and Ag-AgI/Al_2O_3 electrodes.

bution of self-stabilized Ag-AgI/Al_2O_3 were also analyzed based on N_2 adsorption and desorption curves (Fig. 3B), which suggest that Ag-AgI/Al_2O_3 is in adsorption curve of type IV (Brunauer, Deming, Deming, and Teller (BDDT)) and presents with mesopores (~5 nm) [30]. Obviously, after Ag-AgI deposition on Al_2O_3, the BET specific surface area of pure Al_2O_3 decrease from 251.392 to 189.126 m^2/g, and the pore volume of Ag-AgI/Al_2O_3 also decrease from 0.348 to 0.346 cm^3/g, confirming that Ag-AgI particles were highly dispersed on Al_2O_3 surface and even embedded into the inner channel of Al_2O_3.

The microstructure of self-stabilized Ag-AgI/Al_2O_3 after 1 h irradiation were also observed by SEM (Fig. 4), it can be seen that Ag-AgI particles were well dispersed on the surface of Al_2O_3, with the color of Al_2O_3 changed from white to grey yellow. Additionally, the results of EDS analysis indicate the atomic ratio of Ag: I is about 1.26 more than the stoichiometric ratio of AgI, further confirming the existence of excess Ag^0 species and consistent with XPS results.

3.2. Plasmon induced charge transfer of self-stabilized Ag-AgI/Al_2O_3

The charge transfer processes of plasma-induced charges were followed by carrying out the photocurrent-time profiles for self-stabilized AgI/Al_2O_3 and Ag-AgI/Al_2O_3 electrode under VL irradiation (Fig. 5A). It is clearly seen that the transient photocurrent responses have almost the same shape for both electrodes and the uniform photocurrent responses are observed for each light-on and light-off cycle, indicating that the charge transport in AgI/Al_2O_3 and Ag-AgI/Al_2O_3 electrodes proceeds quickly. Especially, much larger photocurrent density was observed in Ag-AgI/Al_2O_3 than

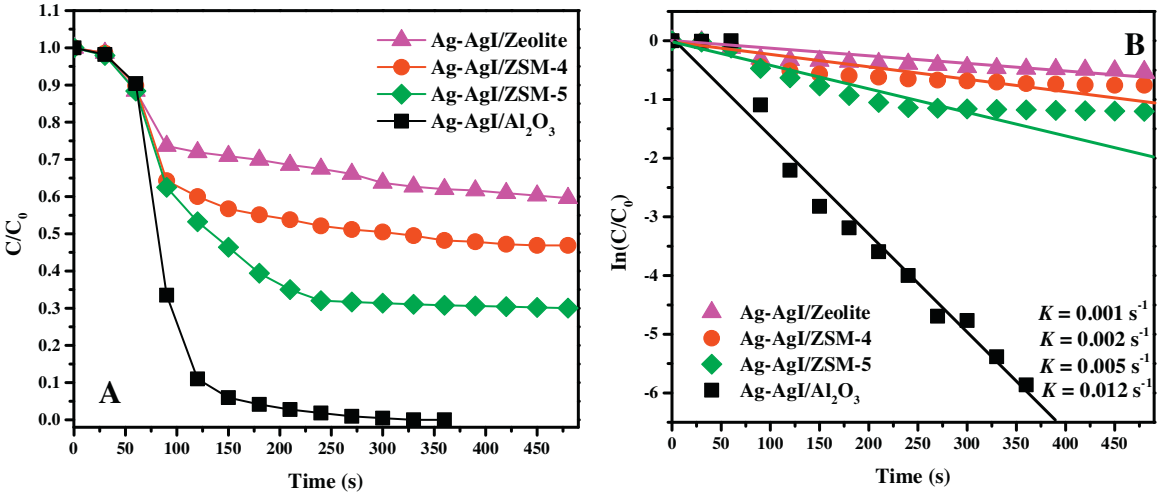

Fig. 6. (A) NO removal rate on different photocatalyst and (B) dependence of $\ln(C/C_0)$ vs. irradiation time ([NO] = 50 ppm, V_{Gas} = 0.16 L min^{-1}).

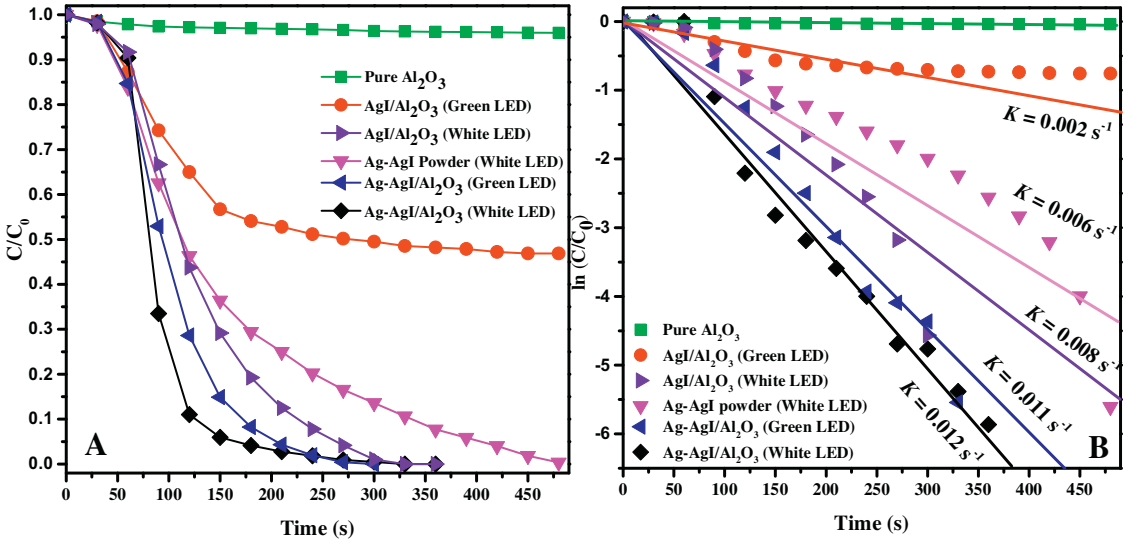

Fig. 7. (A) Plots of NO removal efficiency in the presence of different photocatalyst. ([NO] = 50 ppm, V_{Gas} = 0.16 L min^{-1}), and (B) dependence of $\ln(C/C_0)$ vs. irradiation time.

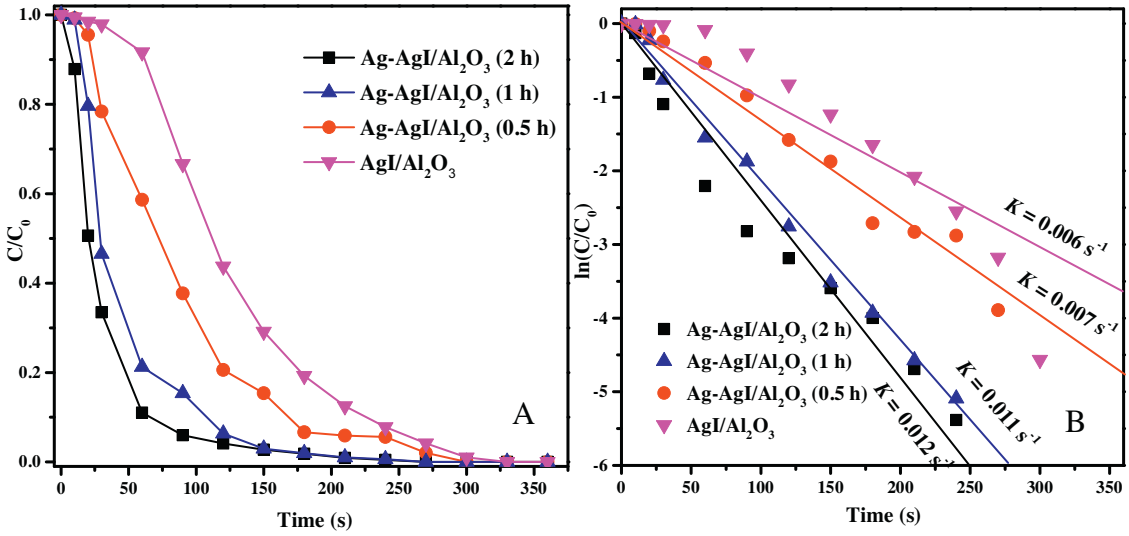

Fig. 8. (A) Plots of NO removal efficiency in the presence of Ag-AgI/Al_2O_3 with different irradiation time ([NO] = 50 ppm, V_{Gas} = 0.16 L min^{-1}), and (B) dependence of $\ln(C/C_0)$ vs. irradiation time.

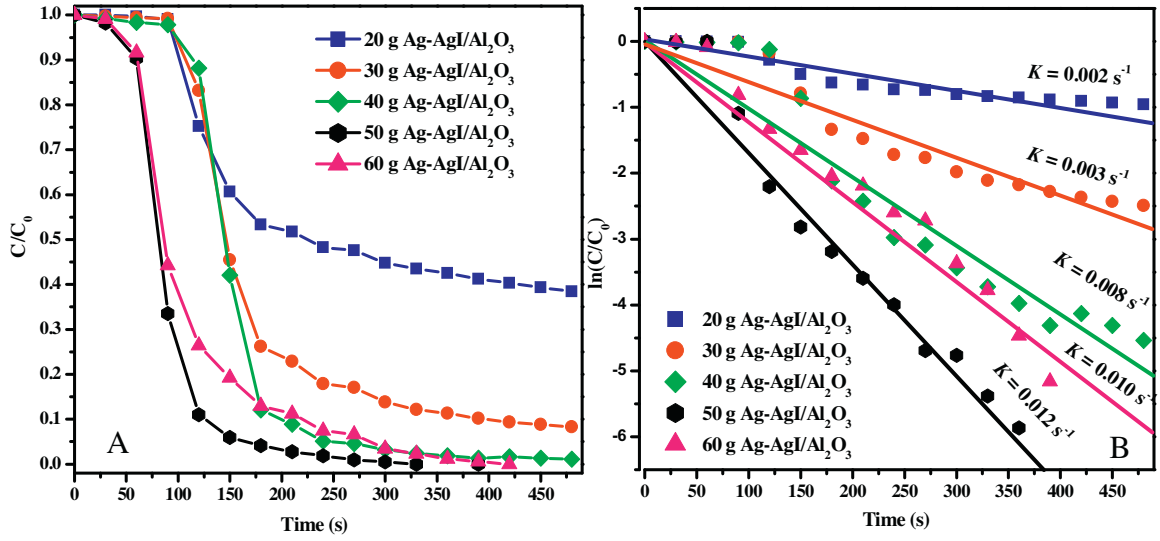

Fig. 9. (A) Effect of Ag-AgI/Al_2O_3 dosage on NO removal rate ([NO] = 50 ppm, V_{Gas} = 0.16 L min^{-1}), and (B) dependence of ln(C/C_0) vs. irradiation time.

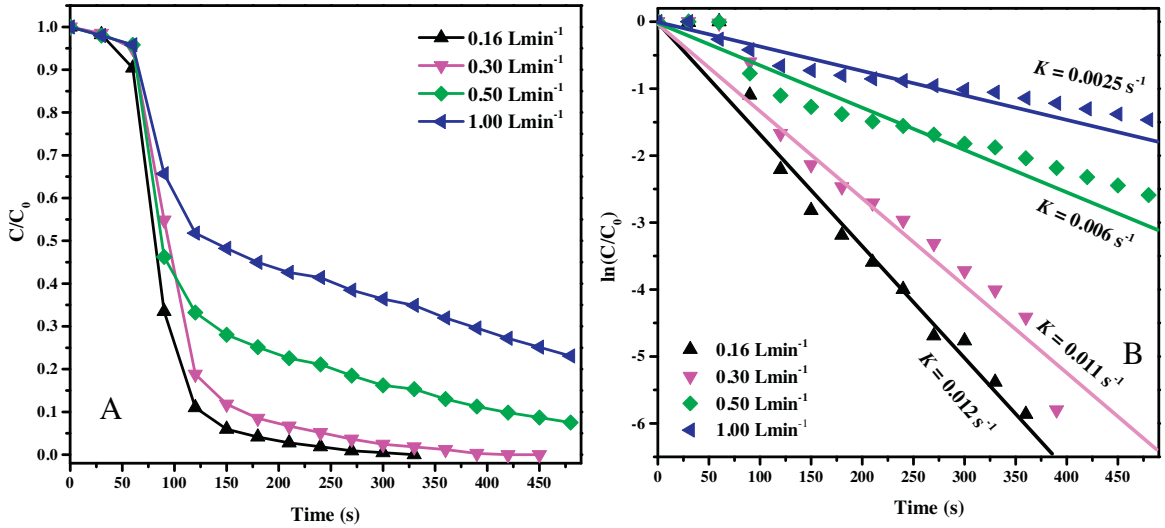

Fig. 10. (A) Effect of NO inlet velocity on NO removal efficiency, and (B) dependence of ln(C/C_0) vs irradiation time.

AgI/Al_2O_3 electrode, mainly attributed to the plasmon effect of Ag NPs [25]. Furthermore, the improved charge separation effect was also confirmed by the electrochemical impedance spectra (EIS) of both electrodes. As shown in Fig. 5B, the Nyquist plot of Ag-AgI/Al_2O_3 electrode is much smaller than that of AgI/Al_2O_3 electrode under VL irradiation, indicating a more effective separation of electron-hole pairs and fast interface charge transfer occurred in Ag-AgI/Al_2O_3. Meanwhile, the plots were fitted with the equivalent circuit (Fig. S2), consisted of charge transfer resistance (R_2), Warburg impedance (W), capacitance (C), and resistance (R_1) [33]. Since the electrolyte and the electrode connection for all samples measurements were the same, therefore, R_1 directly demonstrated the photocatalyst substrate resistance. By fitting the plots of EIS, R_1 and R_2 for AgI/Al_2O_3 and Ag-AgI/Al_2O_3 under dark and VL irradiation were obtained (inset in Fig. 5B). It is obvious that the impedance of Ag-AgI/Al_2O_3 was lower than those of AgI/Al_2O_3 in the charge transfer process. All above results reveal that Ag nanoparticles can act as a photoelectron sinker to facilitate the transfer of photoinduced electrons and retard the recombination of photoexcited electron-hole pairs, thereby improving the photocatalytic ability and stability of nanostructures [17,23,25].

3.3. Plasmon-induced photocatalytic removal of NO by Ag-AgI/Al_2O_3

3.3.1. Effect of different supporter on NO removal efficiency

To search for the optimal supports, different supporter materials (ZSM-5A, ZSM-4A, zeolite, Al_2O_3) were immersed in the same amount of precursors to prepare immobilized Ag-AgI. The photocatalytic activity of as-prepared Ag-AgI on different supporter was evaluated by removal of NO under LED irradiation. As shown in Fig. 6, all the photocatalysts have a certain ability to remove NO gas. Under VL irradiation for 120 s, Ag-AgI/Al_2O_3 has the highest NO removal efficiency of 100%, while Ag-AgI/ZSM-5A, Ag-AgI/ZSM-4A, Ag-AgI/zeolite were 62%, 56%, 43%, respectively. For a clearly quantitative comparison, the Langmuir–Hinshelwood model (L–H) was used to describe the rates of photocatalytic destruction of NO [10]. Herein, the initial photocatalytic degradation of NO was recognized to follow mass-transfer-controlled first-order kinetics approximately as a result of low concentration target pollutants, as evidenced by the linear plot of ln(C/C_0) versus photocatalytic reaction time (t). The initial rate constant of NO degradation over Ag-AgI/Al_2O_3 under VL irradiation is calculated to be 0.012 s^{-1},

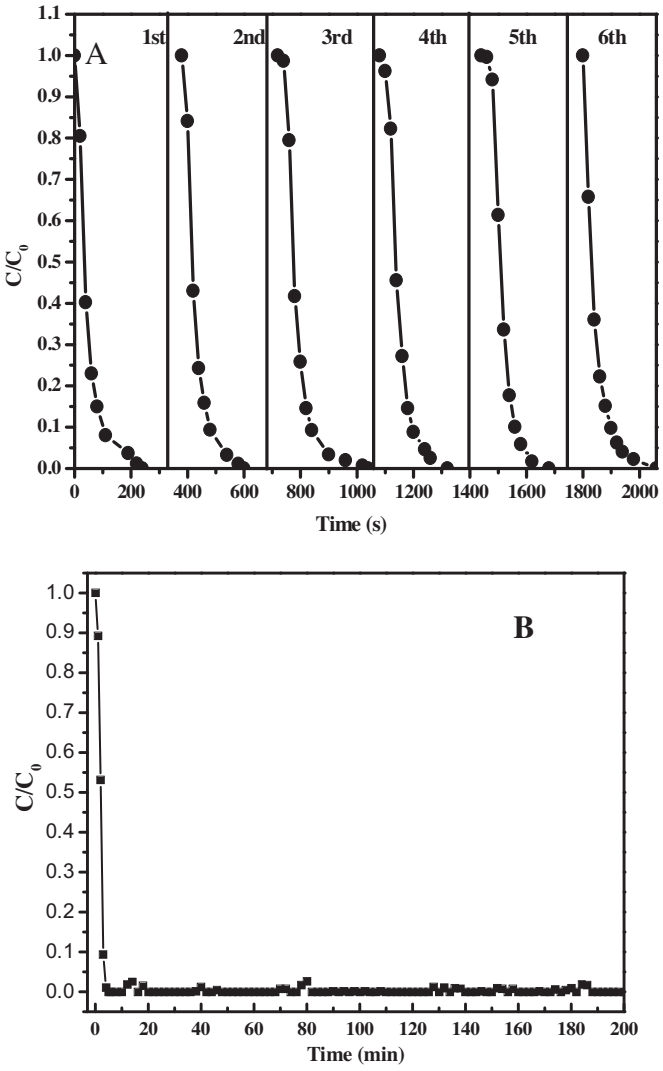

Fig. 11. (A) NO degradation using Ag-AgI/Al_2O_3 in multiple runs, and (B) plots of NO concentration vs. prolonged irradiation time.

faster than other photocatalysts deposited on different supporters. The excellent performance of mesoporous Al_2O_3 supporter can be attributed to its advantages of large surface area (259 $m^2\,g^{-1}$), nanometersized pores (~5 nm), and uniform pore size distribution (Fig. 3B), which could loading more Ag-AgI nanoparticles. Table S1 confirmed that the same amount of different supporter, mesoporous Al_2O_3 could loading almost 2 times amount of Ag-AgI than others. Moreover, the mesoporous architecture of supporter could be able to improve the molecular transport of reactants and products, resulting in a higher quantum efficiency of photocatalytic reaction [32]. Therefore, the mesoprous Al_2O_3 is a suitable supporter for deposition of nanoparticles.

3.3.2. *Effect of plasma Ag-AgI component on NO removal efficiency*

The self-stabilized Ag-AgI/Al_2O_3 was employed for photocatalytic removal of NO under LED irradiation in a continuous mode to demonstrate their potential capability for polluted air purification, as shown in Fig. 7. As a comparison, NO removal was also performed with AgI/Al_2O_3. It was observed that the rate of NO degradation in the presence of Ag-AgI/Al_2O_3 was several times faster than that of AgI/Al_2O_3, when irradiated. Whereas light alone showed none activity for NO removal, indicating no photolysis of NO occurred. It is well-known that AgI has a suitable band gap that can be excited directly by VL (shorter than 450 nm), and the Ag NPs induced plasmon resonance or electron trapping could further enhance its photocatalytic activity [17,23,25]. To confirm this effect, the green LED (495–570 nm) was utilized as alternative VL source for NO removal, as AgI/Al_2O_3 absorb hardly in these wavelengths range. Interestingly, a significant degradation was observed on AgI/Al_2O_3, whereas Ag-AgI/Al_2O_3 exhibited almost the same activity as it did with white LED, further confirming the great SPR effect of Ag nanoparticles, especially with $\lambda > 450$ nm VL irradiation.

Moreover, the as-prepared Ag-AgI/Al_2O_3 samples with different irradiation time were also utilized for NO degradation experiments, and the degradation curves for NO are shown in Fig. 8. Obviously, Ag-AgI/Al_2O_3 after 1 h VL irradiation exhibits almost the same rate constant (0.011 s^{-1}) with Ag-AgI/Al_2O_3 after 2 h VL irradiation (0.012 s^{-1}), which are much higher than Ag-AgI/Al_2O_3 after 0.5 h irradiation with rate constant of 0.007 s^{-1} and AgI/Al_2O_3 with rate constant of 0.006 s^{-1}. This result can be attributed to the different proportion of metallic Ag in the samples, Ag-AgI/Al_2O_3 after 2 h irradiation contains 0.166% of metallic Ag, similar to 0.163% of metallic Ag in Ag-AgI/Al_2O_3 after 1 h irradiation, and much higher than that 0.106% of metallic Ag in Ag-AgI/Al_2O_3 after 0.5 h irradiation and 0.015% of metallic Ag in AgI/Al_2O_3. It has been reported that the formation of more metallic Ag nanoparticles can improve the plasmon resonance absorption of photocatalysts, thereby the great enhancement in the visible light adsorption and better photocatalytic performance occurred for Ag-AgI/Al_2O_3 after 1–2 h irradiation. Therefore, with increasing photoreduction time, the initial improvement of photocatalytic activity was accompanied by the rapid increase of metallic Ag owing to the reduction of Ag^+, while the subsequently stable activity corresponds to the formation of a stable Ag-AgI/Al_2O_3.

Furthermore, different dosage of Ag-AgI/Al_2O_3 was installed into reactor, which exhibit respective photocatalytic activity for NO removal (Fig. 9). Obviously, the content of photosensitive composition Ag-AgI increases with the increase of Ag-AgI/Al_2O_3 dosage, thus, leading to its photocatalytic efficiency due to more generation of photoelectrons and holes. Later, with more addition of Ag-AgI/Al_2O_3, NO removal efficiency attained an equilibrium and no further clear enhancement was observed, this may due to that lots of photocatalyst may induce the light scattering and lower light utilization [34].

3.3.3. *Effect of inlet velocity on NO removal efficiency*

Fig. 10A shows the effect of NO inlet velocity on NO photodegration efficiency using self-stabilized Ag-AgI/Al_2O_3 under LED irradiation. In this experiment, the inlet concentration of NO was controlled at 50 ppm, while the flow rate of NO changed in the range of 0.16–1.00 L min^{-1}. It can be seen that, with an increase of gas flow rate from 0.16 L min^{-1} to 1.00 L min^{-1}, the removal efficiency of NO rapidly decreases from 100% to 66.8%. For a clear quantitative comparison, the Langmuir–Hinshelwood model (L–H) was used to describe the initial rates on photocatalytic removal of NO [10,11]. It can be seen that the initial rate constant of NO removal decrease from 0.012 s^{-1} to 0.0025 s^{-1} (Fig. 10B). This phenomenon can be accounted as follows: the increase in the NO flow means the decrease of NO residence time in the reactor [10–12], resulting in the fleeing of NO molecular without reaction, then led to the low-efficient performance. Herein, a gas flow rate of 0.16 L min^{-1} is optimal for the complete removal of NO.

3.3.4. *Durability of self-stabilized plasma Ag-AgI/Al_2O_3*

The stability and recyclability of photocatalysts are important for practical applications. Under the optimum conditions, the durability of Ag-AgI/Al_2O_3 catalyst was evaluated by continuous photocatalytic removal of NO under LED irradiation. As shown in

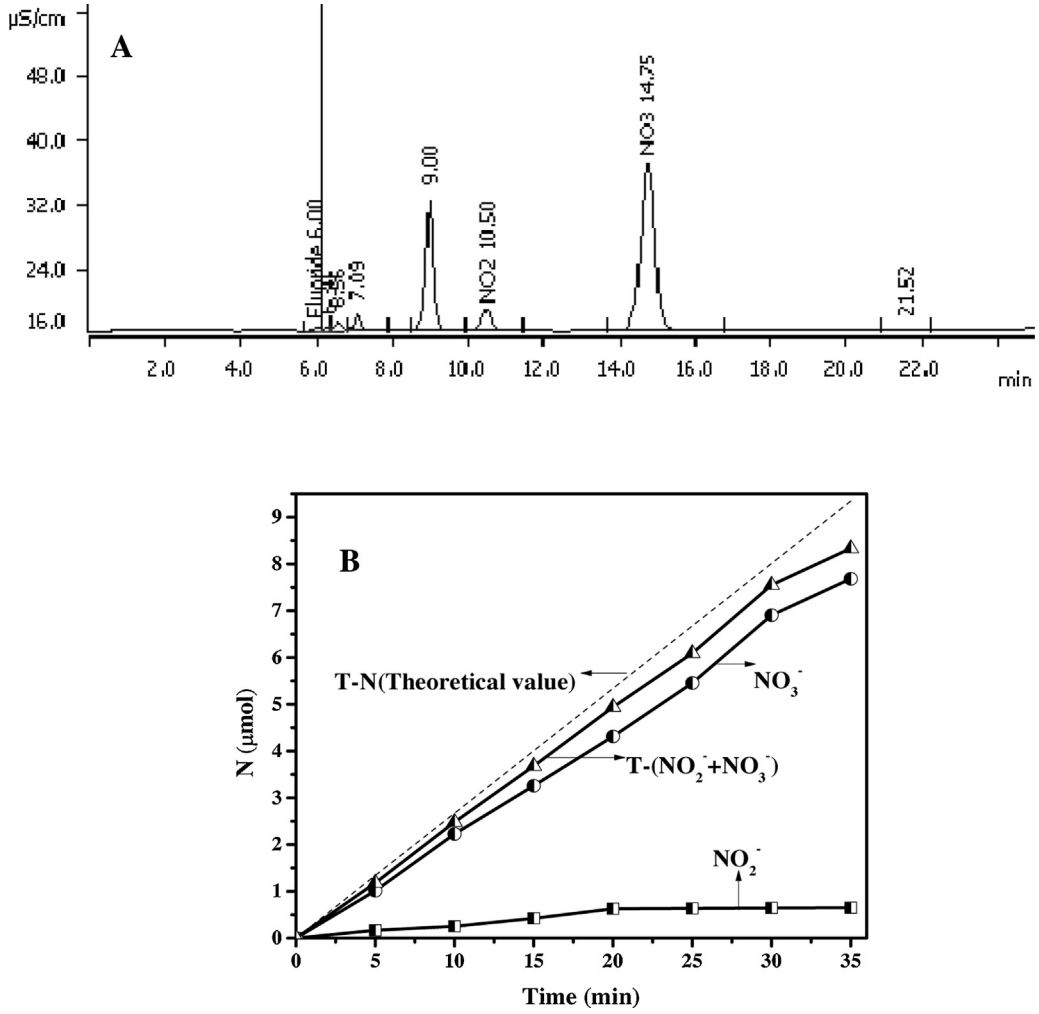

Fig. 12. (A) IC analysis of final photocatalytic products of NO using Ag-AgI/Al_2O_3; (B) Amount of NO_3^- and NO_2^- collected with water during reaction process vs. reaction time.

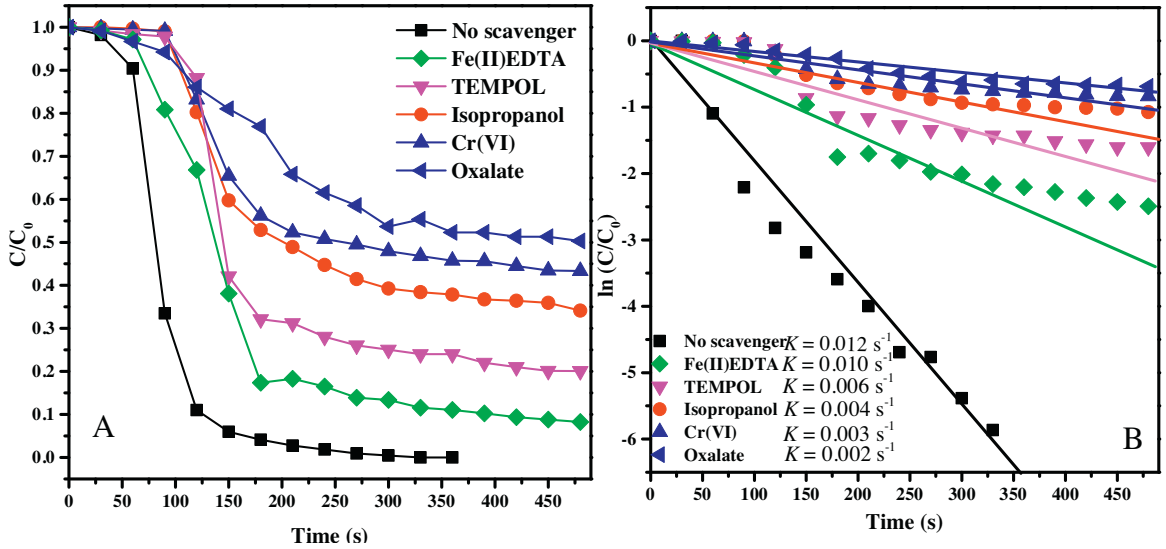

Fig. 13. (A) Curves of NO removal efficiency with addition of several chemical scavenger (isopropanol, sodium oxalate, TEMPOL, Fe(II)-EDTA, $K_2Cr_2O_7$), and (B) plots of NO concentration vs. prolonged irradiation time.

Fig. 11A, it was interesting to find the Ag-AgI/Al_2O_3 still remains high NO removal efficiency even after undergoing 5 repeated runs. In addition, a prolonged continuous 200-min photodegradation experimental result further confirmed that Ag-AgI/Al_2O_3 were not deactivated during the photocatalytic oxidation of ppm-level NO (Fig. 11B), indicating that immobilized Ag-AgI is stable in activity and is promising catalysts for gas purification under visible light irradiation.

The Ag-AgI/Al_2O_3 samples after 5 cycling runs were also collected and analyzed by XRD characterization. It was observed that XRD patterns (Fig. 2A) of the irradiated sample is almost identical to that of the fresh sample, without new peaks (i.e., Ag^0 or I_2) formed, implying the sample is stable in phase structure and AgI phase cannot be destroyed under light irradiation. The XPS results (Fig. 2B) also showed no increase of metallic Ag formation and no change of plasmon absorption at 450–800 nm were also observed in the spectra of UV–vis adsorption.

3.4. Mass analysis of NO during photocatalytic process

To reveal the photocatalytic oxidation process of Ag-AgI/Al_2O_3, the products of NO degradation were quantitatively measured through IC analysis, which each plot was acquired by repeating separated experiments in which the illumination stopped at a given time (Fig. 12). It was found the amount of NO_3^- progressively grew linearly with reaction time and the concentration reached up to 7.682 μmol till 35 min, revealing the continuous production of NO_3^- during the photocatalytic process. Meanwhile, the amount of NO_2^- increases at the initial 15 min, then keeps almost constant at 0.64 μmol regardless of the prolonged illumination. Notably, the amount of produced NO_2^- is much lower than that of produced NO_3^-, indicating that the oxidation of NO to NO_3^- is the major process and the major final product is NO_3^- for the oxidation of gaseous NO over Ag-AgI/Al_2O_3. It has been reported that more NO_3^- would be generated and accumulated with proceeded reaction, which would worsen photocatalytic performance in the later stage [10–12]. However, no significant impact to deactivate Ag-AgI/Al_2O_3 is primary attributed to the special meso/macro pore structure of Al_2O_3 supporter, whose penetrated-pore structure could accommodate more products and postpone lifespan. As known, the open mesoporous/macroporous architecture with large surface area and 3D pores plays an important role in catalyst deposition for its being able to improve the molecular transport of reactants and products [30,32]. Moreover, the total nitrogen-mass balance between the produced NO_3^- and NO_2^- and the supplied NO was calculated. It was found that the total amount of NO_x^- (NO_3^--N + NO_2^--N) determined from IC analysis was almost same with that of the supplied NO amount, indicating all gaseous NO was photocatalytically oxidized.

3.5. Reactive species analysis in Ag-AgI/Al_2O_3 photocatalytic process

Since the reactive oxidative species (ROSs), mainly generated by separation of electron and hole, is the critical role to determine the photocatalytic efficiency, thus, the effect of various radical scavengers on NO removal was examined under LED irradiation. As shown in Fig. 13, it was noted that both photogenerated h^+ and e^- are significantly involved in the reaction, which were evidenced by the great inhibition of NO removal after addition of oxalate (h^+ scavenger) and Cr(IV) (e^- scavenger) in Ag-AgI/Al_2O_3 system. It is well known that ROSs can be produced by two pathways, that is, h_{vb}^+ oxidized water molecules to form ROSs (oxidative pathway), and O_2 captured the photogenerated electron to generate $^{\bullet}O_2^-$ and subsequently produce ·OH (reductive pathway). It can be seen that NO degradation was partly restrained by isopropanol ($^{\bullet}$OH scavenger) with residual of 20 ppm NO, indicating the critical role of the generated $^{\bullet}$OH. Importantly, the further $^{\bullet}$OH probe results obtained with terephthalic acid (0.4 mM) that the increasing fluorescence intensities emits at 440 nm confirm the involvement of $^{\bullet}$OH radicals (Fig. 14A). Similarly, in the presence of TEMPOL ($^{\bullet}O_2^-$ scavenger), there are still 10 ppm NO without removal, suggesting the mod-

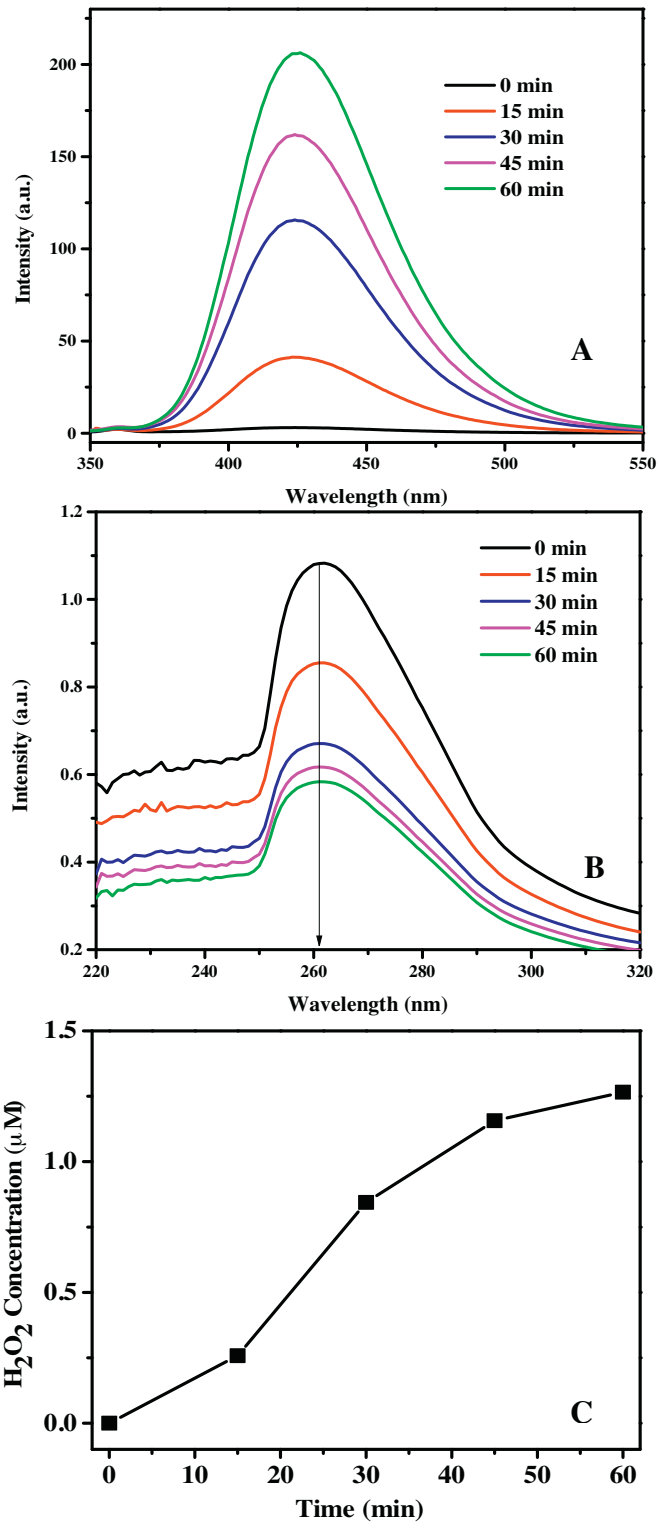

Fig. 14. (A) Time-dependent fluorescence spectra of $^{\bullet}$OH in terephthalic acid solution (4×10^{-4} M); (B) time-dependent degradation of NBT to detect $^{\bullet}O_2^-$ (2.5×10^{-5} M); (C) Accumulation of H_2O_2 produced in photocatalytic process of Ag-AgI/Al_2O_3 under white LED irradiation.

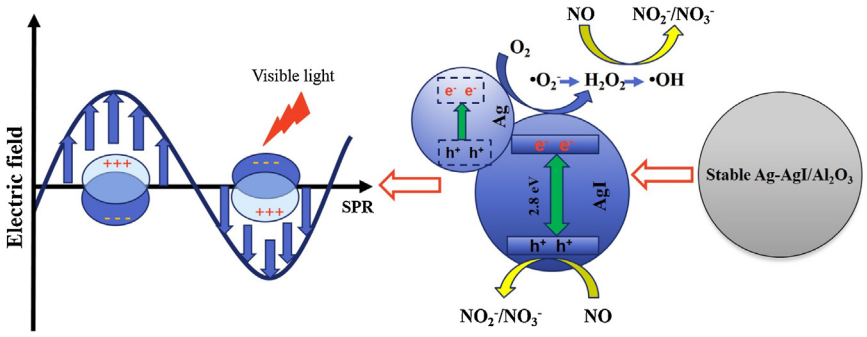

Fig. 15. Scheme for photoexcitation of self-stabilized Ag-AgI/Al_2O_3 under visible light irradiation.

erate role of $^{\bullet}O_2^-$ in the reaction. Meanwhile, NBT sodium salt (0.15 mM), a probe for $^{\bullet}O_2^-$, as indicated by the decrease of absorption at 260 nm after photocatalytic degradation, was also observed upon LED excitation (Fig. 14B). In addition, the slight involvement of H_2O_2 was confirmed by the residual of 6 ppm NO after adding Fe(II)-EDTA (Fig. 13), and its concentration was measured to attain at ca. 3 μM (Fig. 14C).

Theoretically, under VL irradiation, both AgI and Ag NPs can be initiated by the absorption of VL photons, leading to the generation of electron-hole pairs. According to a previous report, the photogenerated holes (+ 1.25 V vs. NHE) in AgI cannot oxidize hydroxyl ion (OH^-) to form $^{\bullet}OH$ since the valence band (VB) of AgI is lower than the standard redox potential of $^{\bullet}OH/OH^-$ (+ 2.38 V vs. NHE); however, h^+ in the VB of AgI with high oxidative potential still can directly oxidize NO molecules and play critical role. Meanwhile, the reduction potential of the conduction band (CB) of AgI is −1.15 V vs. NHE, it is suggested that the electron in the CB from plasmon induced Ag NPs could reduce oxygen to $^{\bullet}O_2^-$ (-0.33 V vs. NHE), and subsequently produce H_2O_2 or $^{\bullet}OH$ [17]. Thus, the generated $^{\bullet}O_2^-$ is an alternative main driving for the photocatalytic oxidation of NO in our present experiment. Moreover, H_2O_2 also can be thermodynamically generated by either two-electron reduction of surface adsorbed O_2 (0.68 V vs NHE) or two-electron oxidation of surface adsorbed H_2O (1.78 V vs NHE) in the CB [29,35]. In conclusion, these facts confirm that $^{\bullet}OH$, $^{\bullet}O_2^-$ and H_2O_2 were generated under VL irradiated conditions, indicating that photogenerated VB-holes (AgI) and plasmonic electrons (Ag NPs) could retain long enough and react with adsorbed oxygen/H_2O to produce a series of ROSs, which finally induce the effective oxidation of NO.

3.6. Possible reaction mechanism of NO removal

It is of significance for the application of SPR photocatalysts to understand photocatalytic mechanisms of such Ag-AgI/Al_2O_3 photocatalyst. When subjected to VL irradiation, Ag-AgI/Al_2O_3 hybrids are excited due to the localized SPR of Ag nanocrystal and generate electron-hole pairs in Ag-AgI nanocrystal. Because the surface of AgI particles is usually terminated by I^- ion and therefore negatively charged, free electrons in metallic Ag nanoparticle deposited on AgI surface are polarized. Under polarization field provided by AgI, the plasmon-excited electrons move and accumulate on the surface of Ag nanocrystal, thus which act as reservoir for photogenerated electrons from AgI and promote the charge separation, thereby enhancing the survived holes on the surface of AgI and oxidize NO molecules [16–22]. Most importantly, Ag NPs act as sinker of photoelectrons could also suppress the decomposition of AgI and the loss of iodine, which ensured the stability of the catalyst performance.

Additionally, the photocatalytic reaction also involves the transportation of NO molecule over catalyst surface. Previous reports have shown the catalyst on mesporous architecture supports could increase the adsorption and pre-concentration for gaseous pollutants [30,32]. Under light irradiation, the pre-concentrated NO molecules over mesporous Ag-AgI/Al_2O_3 surface substantially react with photogenerated active species, which promotes the photocatalytic oxidation of NO. Therefore, the mechanism of removal NO includes of adsorption and photocatalytic oxidation can be illustrated in Fig. 15. That is the following way [17–22].

$$\text{Ag-AgI/Al}_2\text{O}_3 + h\nu \rightarrow e^-(CB) + h^+(VB) \quad (1)$$

$$\text{Ag}(0) + h\nu \rightarrow \text{Ag}(I) + e^- \quad (2)$$

$$\text{Ag}(I) + e^- \rightarrow \text{Ag}(0) \quad (3)$$

$$O_2 + e^- \rightarrow {}^{\bullet}O_2^- \quad (4)$$

$$O_2 + 2H^+ + 2e_{CB}^- \rightarrow H_2O_2 \quad (5)$$

$$H_2O_2 + {}^{\bullet}O_2^- \rightarrow {}^{\bullet}OH + OH^- + O_2 \quad (6)$$

NO can be oxidized by free radicals

$$NO + O_2 + h^+ \rightarrow NO_2 \quad (7)$$

$$NO + {}^{\bullet}OH \rightarrow NO_2 + H_2O \quad (8)$$

$$NO + {}^{\bullet}O_2^- \rightarrow NO_3^- \quad (9)$$

$$NO + H_2O_2 \rightarrow HNO_2/HNO_3 + H^+ \quad (10)$$

4. Conclusion

The self-stabilized Ag-AgI/Al_2O_3 was synthesized by wet impregnation-precipitation and photoreduction method. It is confirmed that self-stabilized Ag-AgI/Al_2O_3 photocatalysts contain hexagonal AgI phase and metallic Ag particles. The large dispersion of Ag-AgI on mesoporous Al_2O_3 can efficiently enhance NO removal efficiency. Most importantly, the plasmonic Ag-AgI/Al_2O_3 photocatalyst was stable and maintained high photocatalytic activity in the repeated test, it can be attributed to the plasmonic structure that photogenerated electron were captured by metallic Ag. In addition, ROSs determination and scavenger study confirm that the responsible ROSs for NO removal is $^{\bullet}OH$, $^{\bullet}O_2^-$ H_2O_2 and h^+.

Acknowledgments

The authors wish to thank the National Natural Science Foundation of China (No. 51578556, 21273085), Natural Science Foundation of Guangdong Province (No. 2015A030308005, S2013010012927, S2011010003416), Science and Technology Research Programs of Guangdong Province (No. 2014A020216009), and the Fundamental Research Funds for the Central Universities (No. 13lgjc10) for financially supporting this work.

Appendix A. Supplementary data

Supplementary data associated with this article can be found, in the online version, at http://dx.doi.org/10.1016/j.apcatb.2015.12.019.

References

[1] A. Farrell, Energy Policy 29 (2001) 1061–1072.
[2] T. Castro, S. Madronich, S. Rivale, A. Muhlia, B. Mar, Atmos. Environ. 35 (2001) 1765–1772.
[3] L.S.R. Brickus, J.N. Cardoso, F.R. De Aquino Neto, Environ. Sci. Technol. 32 (1998) 3485–3490.
[4] S.L. Fischer, C.P. Koshland, Environ. Sci. Technol. 41 (2007) 3121–3126.
[5] I. Heo, M.K. Kim, S. Sung, I.-S. Nam, B.K. Cho, K.L. Olson, W. Li, Environ. Sci. Technol. 47 (2013) 3657–3664.
[6] Q. Guo, T. Sun, Y. Wang, Y. He, J. Jia, Environ. Sci. Technol. 47 (2013) 9514–9522.
[7] W.S. Epling, L.E. Campbell, A. Yezerets, N.W. Currier, J.E. Parks, Catal. Rev. Sci. Eng. 46 (2004) 163–245.
[8] D.H. Xia, C. He, L.F. Zhu, Y.L. Huang, H.Y. Dong, M.H. Su, A.M. Bian, D. Abou, J. Environ. Monit. 13 (2011) 864–870.
[9] X.Y. Wu, S. Yin, Q. Dong, C.S. Guo, T. Kimura, J. Matsushita, T. Sato, J. Phys. Chem. C 117 (2013) 8345–8352.
[10] Z.H. Ai, W. Ho, S. Lee, L.Z. Zhang, Environ. Sci. Technol. 43 (2009) 4143–4150.
[11] G. Li, D.Q. Zhang, J.C. Yu, M.K. Leung, Environ. Sci. Technol. 44 (2010) 4276–4281.
[12] S.X. Ge, L.Z. Zhang, Environ. Sci. Technol. 45 (2011) 3027–3033.
[13] Q. Dong, S. Yin, C. Guo, X. Wu, N.T. Kumada, A. Takei, Y. Miura, T. Yonesaki Sato, Appl. Catal. B 147 (2014) 741–747.
[14] R. Sugraneza, J. Balbuena, M. Cruz-Yusta, F. Martín, J. Moralesa, L. Sánchez, Appl. Catal. B 165 (2015) 529–536.
[15] F. Dong, Z.W. Zhao, T. Xiong, Z.L. Ni, W.D. Zhang, Y.J. Sun, W.-K. Ho, ACS Appl. Mater. Interfaces 5 (2013) 11392–11401.
[16] M.S. Zhu, P.L. Chen, M.H. Liu, ACS Nano 5 (2011) 4529–4536.
[17] C. Hu, T.W. Peng, X.X. Hu, Y.L. Nie, X.F. Zhou, J.H. Qu, H. He, J. Am. Chem. Soc. 132 (2009) 857–862.
[18] Y. Hou, X.Y. Li, Q.D. Zhao, G.H. Chen, C.L. Raston, Environ. Sci. Technol. 46 (2012) 4042–4050.
[19] Y.F. Shen, P.L. Chen, D. Xiao, C.C. Chen, M.S. Zhu, T.S. Li, W.G. Ma, M.H. Liu, Langmuir 31 (2015) 602–610.
[20] S.L. Zhang, K.H. Wong, H.Y. Yip, C. Hu, J.C. Yu, C.Y. Chan, P.K. Wong, Environ. Sci. Technol. 44 (2010) 1392–1398.
[21] H.X. Shi, G.Y. Li, H.W. Sun, T.C. An, H.J. Zhao, P.-K. Wong, Appl. Catal. B 158–159 (2014) 301–307.
[22] H. Zhang, X.F. Fan, X. Quan, S. Chen, H.T. Yu, Environ. Sci. Technol. 45 (2011) 5731–5736.
[23] S.W. Zhang, J.X. Li, X.K. Wang, Y.S. Huang, M.Y. Zeng, J.Z. Xu, ACS Appl. Mater. Interface 6 (2014) 22116–22125.
[24] H. Yu, L. Liu, X. Wang, P. Wang, Y. Jia, Y. Wang, Dalton Trans. 41 (2012) 10405–10411.
[25] P. Wang, B.B. Huang, X.Y. Qin, X.Y. Zhang, Y. Dai, J.Y. Wei, M.H. Whangbo, Angew. Chem. Int. Ed. 47 (2008) 7931–7933.
[26] Z. Zheng, C. Chen, A. Bo, F.S. Zavahir, E.R. Waclawik, J. Zhao, D. Yang, H. Zhu, Chem. Catal. Chem. 6 (2014) 1210–1214.
[27] C. An, J. Wang, J. Liu, S. Wang, Q.H. Zhang, RSC Adv. 4 (2014) 2409.
[28] F. Dong, Z. Wang, Y. Li, W.-K. Ho, S.C. Lee, Environ. Sci. Technol. 48 (2014) 10345–10353.
[29] D.H. Xia, Z. Shen, G. Huang, W. Wang, J.C. Yu, P.K. Wong, Environ. Sci. Technol. 49 (2015) 6264–6273.
[30] D.H. Xia, T.W. Ng, T.C. An, G.Y. Li, Y. Li, H.Y. Yip, H.J. Zhao, A.H. Lu, P.K. Wong, Environ. Sci. Technol. 47 (2013) 11166–11173.
[31] D.H. Xia, Y. Li, G.C. Huang, C.C. Fong, T.C. An, G.Y. Li, H.Y. Yip, H.J. Zhao, A.H. Lu, P.K. Wong, Appl. Catal. B 176–177 (2015) 749–756.
[32] D.H. Xia, L.L. Hu, C. He, W.Q. Pan, T.S. Yang, D. Shu, Chem. Eng. J. 279 (2015) 929–938.
[33] M. Abou Asi, L.F. Zhu, C. He, V.K. Sharma, D. Shu, S.Z. Li, J.N. Yang, Y. Xiong, Catal. Today 216 (2013) 268–275.
[34] Z.H. Ai, W.K. Ho, S.C. Lee, L.Z. Zhang, Environ. Sci. Technol. 43 (2009) 4143–4150.
[35] S.W. Liu, G.C. Huang, J.G. Yu, T.W. Ng, H.Y. Yip, P.K. Wong, ACS Appl. Mater. Interface 6 (2014) 2407–2414.